SIMPLE RULES FOR CAVITATION INSTABILITIES IN TURBOMACHINERY

Yoshinobu Tsujimoto

Engineering Science, Osaka University
1-3 Machikaneyama, Toyonaka, Osaka, 560-8531, Japan
tujimoto@me.es.osaka-u.ac.jp

Abstract

The present paper focuses on the correlation of cavitation instabilities in turbomachinery with steady cavity length, or a parameter $\sigma/2\alpha$. A linear stability analysis shows that various types of cavitation instabilities start to occur when the steady cavity length becomes larger than 65% of the blade spacing. Experimental evidence for this will be reviewed. If we apply this rule in a cross flow plane, the effects of leading edge sweep to suppress cavitation instabilities can be reasonably explained by using a corrected parameter in cross flow. This will also be addressed.

1. INTRODUCTION

Cavitation instabilities are one of the major concerns for high-speed turbomachinery, such as turbopumps for rocket engines. Following the observation of oscillating cavitation by Acosta (1958), extensive studies have been made mainly from the viewpoint of system instability.

For the system instability, cavities are generally modeled using the factors called cavitation compliance and mass flow gain factor. Various attempts have been made to evaluate those parameters, mainly at Caltech, including Brennen and Acosta (1973), Kim and Acosta (1975), Brennen and Acosta (1976), Brennen (1978), Acosta and Furuya (1979), Brennen et al. (1982). In an attempt to evaluate those parameters based on an unsteady linear cavitating flow analysis, Otsuka et al. (1996) found numerically that those parameters are functions of $\sigma/2\alpha$, where σ is the cavitation number and α is the incidence angle, although the proof for this was made later by Watanabe et al. (1998). As shown by Acosta (1955), the cavity length on a hydrofoil depends on $\sigma/2\alpha$. Therefore, the unsteady cavitation characteristics can be represented as functions of steady cavity length. Although rotating cavitation can be predicted by modeling cavitation by those parameters (Tsujimoto et al., 1993), more detailed cavitating flow analyses are needed for the understanding of local instabilities such as rotating cavitation.

A linear stability analysis of cavitating flow around hydrofoils and cascades was carried out by Watanabe et al. (1998), based on an unsteady linear closed cavity model. This analysis shows that the frequency and amplifying rate of cavitation instabilities depend on $\sigma/2\alpha$, or the steady cavity length. Although the model assuming an infinitesimal disturbance failed to predict cavitation instabilities for an isolated foil, a time marching calculation allowing finite amplitude of oscillation (yet assuming linear closed cavities) favorably simulated the cavitation instabilities for isolated foil (Watanabe et al., 2000). On the other hand, Horiguchi et al. (2000A) have shown that various types of cavitation instabilities start to occur when the steady cavity extends over 65% of blade spacing. Those instabilities can be physically explained by the interaction of the local flow near the cavity closure with the leading edge of opposing blade. If we apply this rule in a cross flow plane, the effects of leading edge sweep to suppress cavitation instabilities can be reasonably explained by using a corrected parameter in cross flow (Acosta et al., 2000).

Motivated by Acosta's correlation of steady cavity length with $\sigma/2\alpha$, attempts to correlate cavitation instabilities with this parameters are carried out by Pham, Larrarte and Fruman (1998) and Arndt, et al. (1998) for

isolated hydrofoils.   Clear correlation of this parameter with Strouhal number is shown in Arndt, et al. (2000) and Kjeldsen, et al. (2000).   Research on isolated hydrofoils will be reviewed by Jean-Pierre Franc in the present Symposium and it will not be detailed here.

   Although the correlation of cavity instabilities with $\sigma/2\alpha$ is derived from linear analysis, it applies reasonably to many practical cases.   The present paper focuses on such correlations observed in turbomachinery.

2. ANALYTICAL METHOD

2.1 Formulation

  We consider a cascade as shown in Fig.1. For simplicity, we assume that downstream conduit length is infinite and no velocity fluctuation occurs there.   The upstream conduit length is assumed to be finite, *L*, in *x* -direction and the conduit is connected to a space with constant (static = total) pressure at the inlet AB.   This is intended to determine if the predicted instability is system dependent or not.   Since we consider a rotor, we assume that the velocity fluctuation at the inlet AB is normal to the cascade axis.   For a stator it is only necessary to assume that the velocity fluctuation is in the direction of the free stream.

   We assume small disturbances with time dependence $e^{j\omega t}$ where $\omega = \omega_R + j\omega_I$ is the complex frequency with ω_R the frequency and ω_I the damping rate, to be determined from the analysis.   The velocity disturbance is represented by a source distribution $q(s_1)$ on the cavity region, vortex distributions $\gamma_1(s_1)$ and $\gamma_2(s_2)$ on the blades, and the free vortex distribution $\gamma_t(\xi)$ downstream of blades, shed from the blades associated with the blade circulation fluctuation.   We define the strength of these singularities using a coordinate fixed to the cavity to take account of cavity length fluctuation.   If we divide the strength of those singularities and the cavity length into steady and unsteady components, we can represent the velocity with steady uniform velocity ($U,U\alpha$), the steady disturbance (u_s,v_s), and the unsteady disturbance ($\tilde{u},\tilde{v}$):

$$u = U + u_s + \tilde{u}e^{j\omega t}$$
$$v = U\alpha + v_s + \tilde{v}e^{j\omega t} \tag{1}$$

We assume that $\alpha \ll 1$, $|\tilde{u}|,|\tilde{v}| \ll |u_s|,|v_s| \ll U$ and neglect higher order small terms.

2.2 Boundary conditions and stability analysis

   The boundary   conditions   are
   1.   The pressure on the cavity should equal vapor pressure.
   2.   The normal velocity on the wetted blade surface should vanish.
   3.   The cavity should close at (moving) cavity trailing edge.
   4.   The pressure difference across the blades should vanish at the blade trailing edge (Unsteady Kutta's
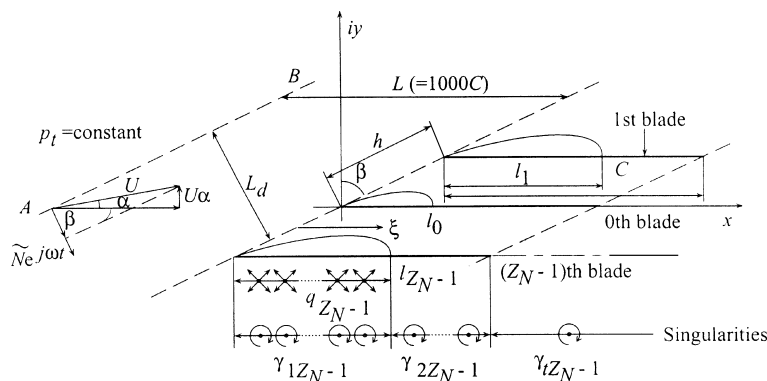

Fig. 1 Flow model for stability analysis

condition).

5. Upstream and downstream conditions: Since the downstream flow rate fluctuation is suppressed owing to the infinite conduit length, the cavity volume fluctuation is related to the upstream fluctuation. The direction of the velocity fluctuation at the inlet AB is assumed as mentioned before.

By specifying the strength of the singularity distributions at discrete points (S_{ij}) on the coordinates fixed to the fluctuating cavity as unknowns, we can represent the boundary conditions as follows.

For the steady component

$$
A_s(l_s)
\begin{Bmatrix}
q_s(S_{11})/U\alpha \\
: \\
\gamma_1(S_{11})/U\alpha \\
: \\
\gamma_2(S_{11})/U\alpha \\
: \\
\sigma/2\alpha
\end{Bmatrix}
= \{B_s\}
\tag{2}
$$

and for the unsteady component

$$
A_u(l_s,\omega)
\begin{Bmatrix}
\tilde{q}(S_{11}) \\
: \\
\tilde{\gamma}_1(S_{11}) \\
: \\
\tilde{\gamma}_2(S_{11}) \\
: \\
\tilde{u}_c \\
\alpha\tilde{l} \\
\tilde{N}
\end{Bmatrix}
= \{0\}
\tag{3}
$$

where $A_s(l_s)$ and $A_u(l_s,\omega)$ are coefficient matrices, B_s is a constant vector. The steady flow can be determined from Eq. (2), which shows that the steady cavity length l_s is a function of $\sigma/2\alpha$. Equation (3) is a set of linear homogeneous equations. For the cases with externally forced disturbances such as inlet pressure or flow rate fluctuations, we would have a non-zero vector on the right hand side representing the forced disturbances. For the present cases without any external disturbances, the determinant of the coefficient matrix $[A_u(l_s,\omega)]$ should equal zero

$$
|A_u(l_s,\omega)| = 0
\tag{4}
$$

so that we have non-trivial solutions. The complex frequency $\omega = \omega_R + j\omega_I$ is determined from this relation. This equation shows that the frequency ω_R and the damping rate ω_I as well as possible mode of instability depend only on the steady cavity length l_s, or equivalently on $\sigma/2\alpha$, once the geometry and other flow conditions are given.

3. EXAMPLES OF THE CORRELATION OF $\sigma/2\alpha$ WITH INSTABILITIES

Before going into a detailed examination, several examples of the correlation are presented. Figure 2 shows a map of various oscillating cavitation types observed in a three bladed inducer (Tsujimoto et al., 1997) represented on

a suction performance plot. The lines with constant $\sigma/2\alpha$ are drawn in the figure. It can be found that the boundaries between the cavitation types are nearly parallel to the constant $\sigma/2\alpha$ curves.

The next example is a surge instability of a marine propeller tested in a cavitation tunnel (Duttweiler and Brennen, 2000). Figure 3 shows the occurrence of the instability in a cavitation number and advance ratio map. Since the angle of attack in the vicinity of a propeller blade tip is approximately proportional to the difference, $J_0 - J$, between the design advance ratio J_0 and the operating advance ratio J, a particular value of the parameter $\xi = (J_0 - J)/\sigma$ corresponds to a particular value of $\sigma/2\alpha$. Several lines of constant ξ are plotted in Fig.3 where it is clear that the transition between stable and unstable behavior corresponds quite closely to the particular value of $\xi = 2.0$. Thus the instability boundary corresponds to a particular configuration of steady cavity length on the propeller blade.

The third example is the rotating cavitation in a centrifugal impeller of low specific speed (Friedriches and Kosyna, 2001). Figure 4 shows the suction performance curve in which the occurrence of rotating cavitation is also shown. The onset conditions of the rotating cavitation at various flow rates are correlated with $\sigma/2\alpha$ in Table 1. This clearly shows that the rotating cavitation starts to occur at $\sigma/2\alpha \approx 2.34$.
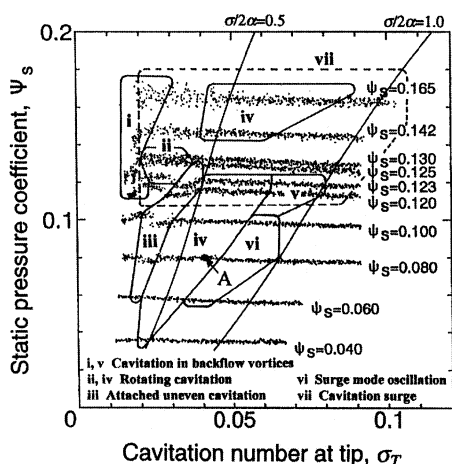

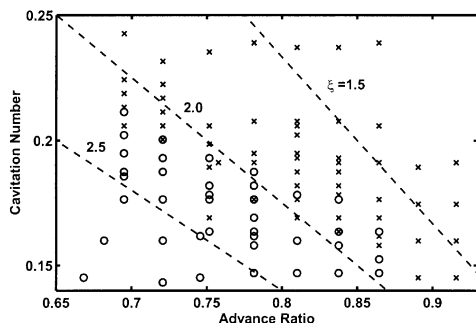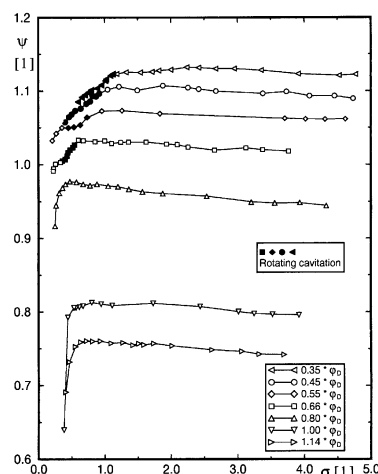Fig. 2 Map of various oscillating cavitation types observed in a 3-bladed inducer, from Tsujimoto et al., 1997

Fig. 4 Occurrence of rotating cavitation shown in a suction performance curve of a centrufugal pump of low specific speed, from Friedriches and Kosyna, 2001

Fig. 3 Occurrence of instability in a cavitation number and advance ratio map, for a marine propeller tested in a cavitation tunnel. Each operating point is classified as stable ($\times$), unstable ($\bigcirc$), or marginally stable ($\otimes$). The propeller rotating speed in this case was n=30.8 Hz. The dash lines (---) are for different values of the parameter ξ, and correspond to the stability criterion discussed in the text, from Duttweiler and Brennen, 2000

Table 1 Onset of rotating cavitation described by $\sigma/2\alpha$ from Friedriches and Kosyna, 2001

Flow rate	$\sigma_{I,Rot}$	α	$\sigma_{I,Rot}/2\alpha$
$0.35 * \varphi_D$	1.13	14.0^o	2.31
$0.45 * \varphi_D$	0.94	11.5^o	2.34
$0.55 * \varphi_D$	0.78	9.5^o	2.35
$0.66 * \varphi_D$	0.53	6.5^o	2.34
$0.80 * \varphi_D$	(0.33)	4.0^o	(2.33)

The above examples show that $\sigma/2\alpha$, or the steady cavity length, controls the onset of cavitation instabilities in various types of machines.

4. ALTERNATE BLADE CAVITATION AND RESULTS OF STABILITY ANALYSIS

It is well known that alternate blade cavitation, in which the cavity length differs alternately, may occur for inducers with an even number of blades. It was found possible to simulate alternate blade cavitation by simply allowing the cavity length to be different on each blade (Horiguchi et al., 2000A). The steady cavity length obtained by assuming equal cavities is plotted in the upper part of Fig.5 (a). The cavity lengths of alternate blade cavitation thus obtained are shown in the upper part of Fig.5 (b), for a cascade with the stagger $\beta = 80$ deg and the chord-pitch ratio $C/h = 2.0$, typical for pump inducers (Horiguchi et al., 2000B). In this calculation, a periodicity over 4 blades is assumed and hence it corresponds to the case of 4-bladed inducer . The alternate blade cavitation starts to develop when the cavity length, l_s, of equal cavitation exceeds 65% of the blade spacing, h.

The flow field around alternate blade cavitation is shown in Fig.6, with those around shorter equal length cavities. We should note that there exists a region near the trailing edge of cavities in which the flow is inclined towards the suction surface of the blades and the incidence angle to the neighboring blade is smaller. This region starts to interact with the leading edge of the neighboring blade when the cavity length exceeds 65% of the blade spacing. If the cavity on one blade becomes longer than 65% of the blade spacing for some reason, the incidence angle to the neighboring blade will decrease and hence the cavity length on the neighboring blade will also decrease. Then the incidence angle to the original blade will increase and the length of the cavity on it will increase further. This is the mechanism of the development of alternate blade cavitation.

The Strouhal numbers $St = \omega_R l_s / 2\pi U$ of various amplifying modes are shown in the lower part of Fig.5 (a) and (b) for equal length cavitation and alternate blade cavitation. The symbol $\theta_{n,n+1}$ shows the phase advance of the disturbance on the upper blade (n+1) with respect to that on the lower blade (n) by one pitch, which is determined from the stability analysis. It is interesting to note that the Strouhal number based on the steady cavity length is kept nearly constant against $\sigma/2\alpha$ for all modes. Here we focus on Mode I. For Mode I, the frequency is zero and the phase difference $\theta_{n,n+1}$ is 180 deg, corresponding to exponential transitions between equal and alternate blade cavitation. This mode appears for equal cavitation longer than 65% of the blade spacing, h, which shows

(a) Steady cavity length and Strouhal numbers
for equal length cavitation

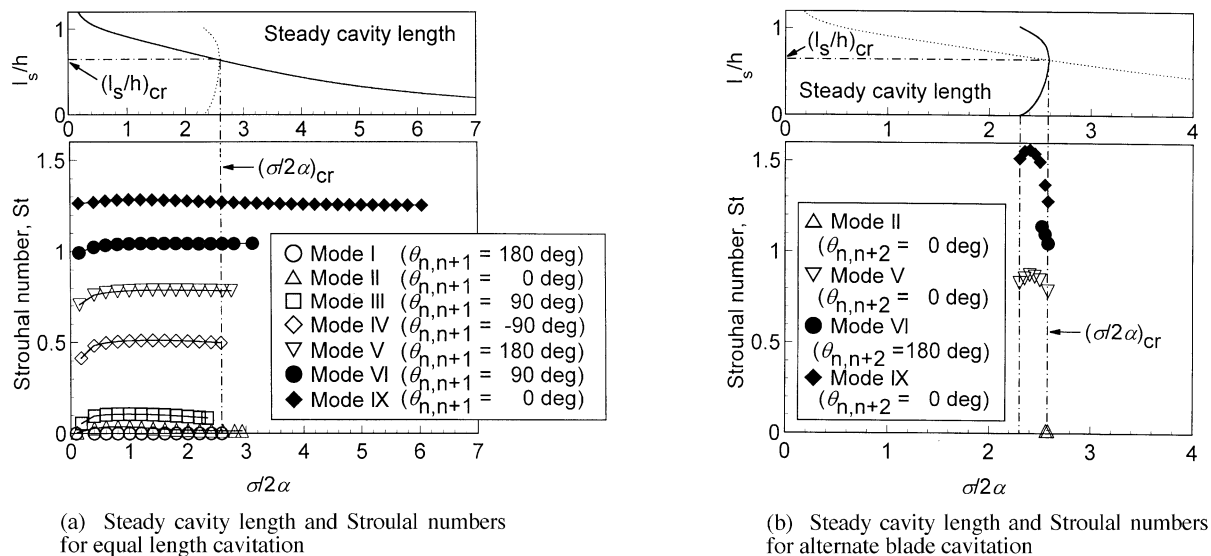(b) Steady cavity length and Strouhal numbers
for alternate blade cavitation

Fig. 5 Steady cavity length (upper figures) and Strouhal numbers
(lower figures) of various unstable modes, for 4-bladed inducer with
C/h=2.0, β =80 deg and L/C=1000, from Horiguchi et al., 2000B

that the longer equal cavitation is statically unstable to a disturbance corresponding to the transition to alternate blade cavitation.   The alternate blade cavitation does not have this mode and hence it is statically stable.   The above discussion applies only for the cases with even number of blades.   With odd number of blades, we do not have a solution corresponding to alternate blade cavitation.   The equal length cavity is statically stable for all values of $\sigma/2\alpha$.

Various unstable modes start to occur for cavities longer than 65% of the blade spacing for which alternate blade cavitation will develop.   This suggests that the mechanism described above for alternate blade cavitation can be the reason also for other instabilities.   Those instabilities are discussed later after examining the "65% spacing" rule.

(a) Equal length cavitation
($\sigma/2\alpha$=7.0, l_s/h=0.202)

(b) Equal length cavitation
($\sigma/2\alpha$=2.58, l_s/h=0.640)

(c) Alternate blade cavitation
($\sigma/2\alpha$=2.58, l_s/h=0.249 and 0.882)
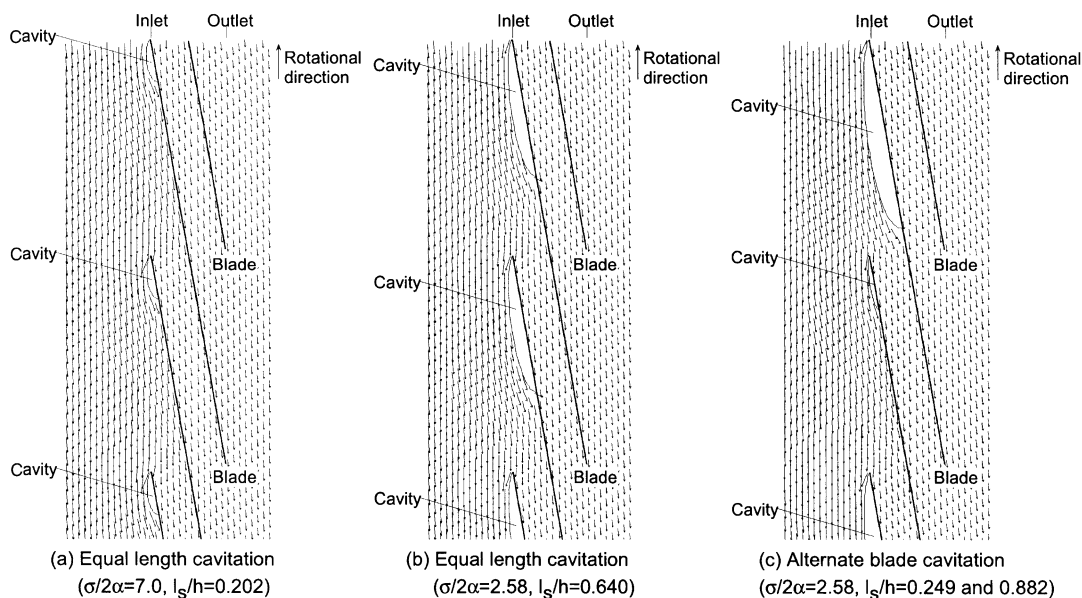
Fig. 6 Steady cavity shape and velocity in the cascade
with C/h=2.0 and in the case with α =4 deg.

5. SWEEP EFFECTS AND EXAMINATION OF 65% SPACING RULE

It is well known that leading edge sweep has a favorable effect on the cavitation of turbomachines.   However, the mechanisms of the improvement have not been made clear.   A cavitation correlation obtained by considering the velocity component in a plane normal to the leading edge is discussed here (Acosta et al., 2000).   Figure 7 shows the cascade with the sweep angle λ measured from the inducer axis.   Velocity triangles in various planes are shown in the figure.   Here, we attempt to correlate the flow in the "Plan view" with that in the "Cross flow plane" which is normal to the leading edge.   We assume that the flow in the cross flow plane is independent of the location of the cross flow plane considered.   First, from geometrical relations, we obtain the following incidence angle α_c in the cross flow plane.

$$\alpha_c = tan^{-1}(tan\alpha/sin\lambda) \approx \alpha/sin\lambda \qquad (5)$$

Second, from the Bernoulli's equation in the "Plan view" we can determine the cavitation number σ_c in the cross flow plane as follows:

$$\sigma_c = \sigma/(cos^2\alpha \, sin^2\lambda + sin^2\alpha) \approx \sigma/sin^2\lambda \qquad (6)$$

The last expressions of Eq. (5) and (6) are obtained for the cases of small α, and $\sigma \equiv (p_1 - p_v)/(\rho V_1^2/2)$ and $\sigma_c \equiv (p_1 - p_v)/(\rho V_{kc1}^2/2)$ are cavitation numbers in the "Plan view"   and   "Cross flow plane" respectively.

Combining Eq. (5) with Eq. (6) we obtain

$$\sigma_c/2\alpha_c = (\sigma/2\alpha)/sin\lambda \qquad (7)$$

This shows that the value of $\sigma/2\alpha$ in the cross flow plane is increased by a factor of $(1/sin\lambda)$. This scaling rule has been successfully applied to the lift and drag coefficients of cavitating single foil by Ihara et al., (1989). Here we examine this rule for the cavitation development in a real inducer. Strictly speaking, the geometry of the cascade in the cross flow plane depends on the sweep angle. This effect is totally neglected here.

The geometry of the inducers tested is shown in Fig.8. They have helical blades with the same camber line and a straight part near the leading edge. So, they have the same inlet and outlet blade angles and the non-cavitating performance is nearly the same for all of the inducers. The cavity lengths for those inducers are plotted against cavitation number σ in Fig. 9 for various flow coefficients. It is evident that the cavity development is delayed significantly for the forward (F30) and backward (B50) swept inducers as compared with the unswept (0) inducer. For all cases, the alternate blade cavitation starts to occur when the cavity length l becomes about 65% of the blade spacing h, as predicted by the analysis. Then the same data is replotted against $\sigma/2\alpha$ in Fig. 10. The cavity development becomes nearly the same for different flow coefficients but we still have the difference among inducers with different sweep. Figure 11 shows the plot against $\sigma_c/2\alpha_c$. Here, the cavity development is nearly the same for all the inducers.
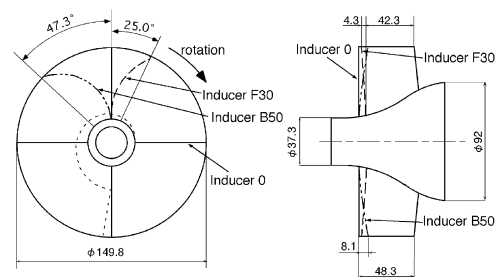

Fig. 8 Geometry of leading edges of test inducers (The leading edge profiles of F30 and B50 are shown only for one blade)

Fig. 7 Geometry of swept cascade, from Acosta et al., 2000

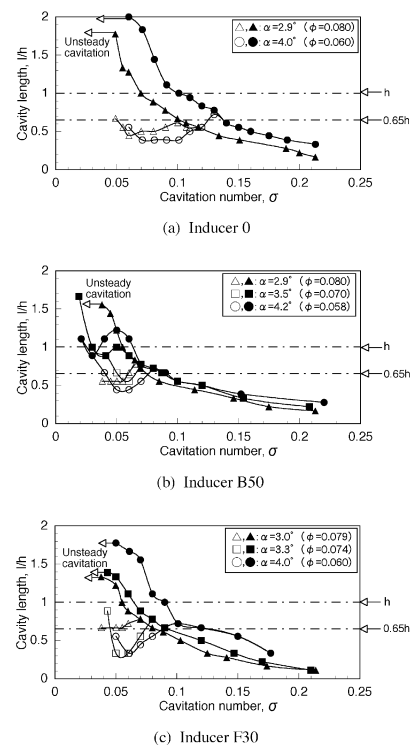
(a) Inducer 0

(b) Inducer B50

(c) Inducer F30

Fig. 9 Plot of cavity length against σ

Among these inducers, we did observe differences in the secondary flow and backflow but the differences were not so large as expected. Figure 11 may suggest that the suction performance improvement by the leading edge sweep is mainly caused by the cross flow effect and it can be represented by a simple parameter $\sigma_c/2\alpha_c$.

For all cases, unsteady cavitation starts to occur when the shorter cavity first shortens and then increases to 65% of the blade spacing. This cannot be explained by the stability analysis but it suggests that the value of $\sigma_c/2\alpha_c$ controls not only steady cavity length but also cavitation instabilities.

(a) Inducer 0

(b) Inducer B50

(c) Inducer F30
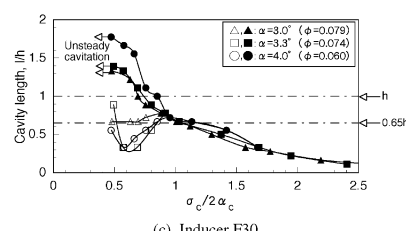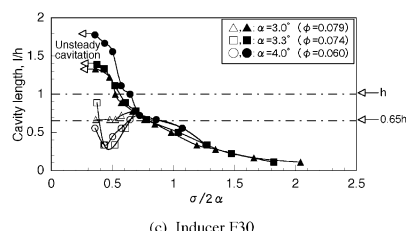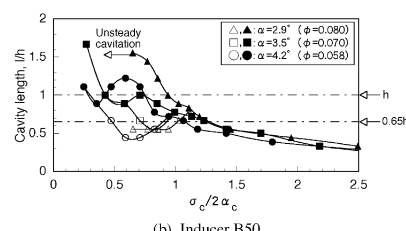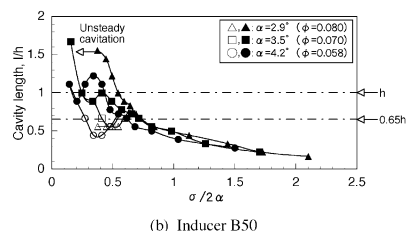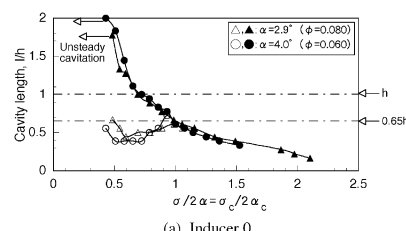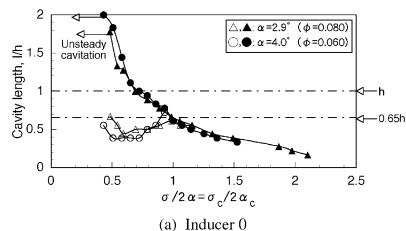
Fig. 10 Plot of cavity length against $\sigma/2\alpha$

(a) Inducer 0

(b) Inducer B50

(c) Inducer F30

Fig. 11 Plot of cavity length against $\sigma_c/2\alpha_c$

6. VARIOUS MODES OF OSCILLATING CAVITATION

We now return to Fig. 5 (a). Mode II is a surge mode oscillation without interblade phase difference: $\theta_{n,n+1} = 0$. It was found that the frequency of this mode correlates with $1/\sqrt{L}$ where L is the length of the upstream conduit. So this mode represents conventional cavitation surge. Only Mode II is system dependent and all other modes are system independent. Mode IX is also a surge mode oscillation with no interblade phase difference but it has higher frequency. This mode is herein called "higher order surge mode oscillation". The cavity volume fluctuation is much smaller than that of conventional cavitation surge, Mode II (Horiguchi et al., 2000B). For this reason the frequency does not depend on the inlet conduit length. In addition, the frequency of this mode does not depend on the geometry of cascade and this mode occurs also for single hydrofoils (Watanabe et al., 1998). However, the Strouhal number 1.3 is significantly larger than that observed for single hydrofoils (0.1-0.3, as in Arndt et al., 2000). This mode starts to appear at much larger values of $\sigma/2\alpha$ than other modes.

Modes III-VI are various modes of rotating cavitation with various interblade phase differences. For Mode III, the phase of disturbance on the upper blade advances by 90 deg, which means that one cell of disturbance per 4 blades rotates around the rotor in the direction of impeller rotation (downward, in Fig.1) relative to the blades. Observed from a stationary frame, the disturbance of Mode III rotates around the rotor with an angular velocity higher than impeller speed. This is conventional rotating cavitation. In the same way, Mode IV represents one-cell rotating cavitation propagating in the opposite direction as the impeller rotation, called "backward rotating

cavitation". Mode V represents 2-cell rotating cavitation :the cavities are just oscillating with 180 deg interblade phase difference but it can be viewed also as a result of two cells rotating either forward or backward. This mode does not appear for inducers with odd number of blades. Mode VI is one-cell forward rotating cavitation with larger propagating speed than Mode III and this mode is called "higher-order rotating cavitation".

All modes except for Mode IX start to occur when the cavity length exceeds 65% of the spacing. So, those modes might be caused by the interaction of the local flow near the cavity trailing edge with the leading edge of the opposing blade, as was explained for alternate blade cavitation. Mode IX occurs for much shorter cavities and no physical explanation has been given so far. Although only Mode III (conventional rotating cavitation) is generally observed, examples of other modes are introduced in the following sections.

6.1 Conventional Rotating Cavitation (Mode III)

Figure 12 compares the propagation velocity ratio, defined as the ratio of the rotational speed of the disturbance in the absolute frame to the rotational speed of the impeller, plotted against the cavitation number at the tip (Watanabe et al., 1999). We observe that

(1) 4-bladed inducers have higher propagation velocity ratios than 3-bladed inducers, and

(2) the propagation velocity ratio decreases as we decrease the cavitation number.

The above tendencies are well simulated by the model. However, the onset range predicted is much larger in terms of the cavitation number. Figure 13 shows the plot of cavity length at the tip for a 3-bladed inducer at various flow coefficients (design point is $\phi = 0.078$), with the onset point of rotating cavitation. Rotating cavitation starts to occur when the cavity length reaches about 70% of the spacing. So, in this case, the cavity length is more useful than $\sigma / 2\alpha$ for the prediction of rotating cavitation.

6.2 Backward Rotating Cavitation (Mode IV)

Backward travelling rotating cavitation was identified for the first time by Hashimoto et al. (1997). Figure 14 shows the spectrum of inlet pressure fluctuation of a 3-bladed inducer rotating at $f_N = 117Hz$. Component F with $f_F = 138Hz$ is conventional forward propagating rotating cavitation. With this component, an additional component with $3(f_F - f_N)=64Hz$, which is the frequency at which the blades cut the cavitating region, is observed. At the cavitation number slightly larger than the forward rotating cavitation onset, Component B with $f_B = 159Hz$ is observed. With this component, an additional component with $3(f_B + f_N) = 828Hz$ is observed. This frequency is obtained if we assume that the cavitated region rotates in the direction opposite to the impeller rotation. Observation of cavity oscillation by high-speed film also suggests backward rotation. Figure 15 compares the propagation velocity ratio, predicted and observed. It is not unreasonable to correlate the observed rotating
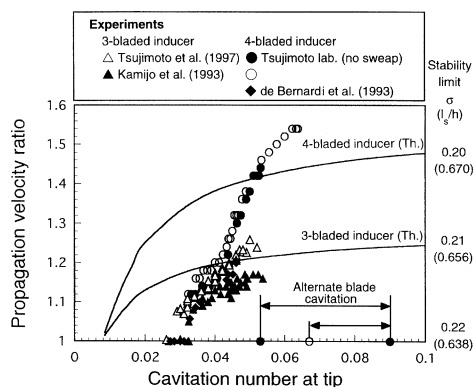

Fig. 12 Comparison of Mode III with conventional rotating cavitation, from Watanabe et al., 1999
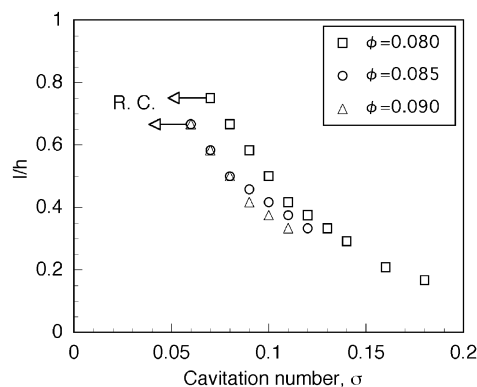
Fig. 13 Cavity length and rotating cavitation onset point for a 3-bladed inducer

cavitation and Mode IV predicted.

Another example of backward rotating cavitation was obtained during the tests of a forward swept 4-bladed inducer similar to F30 in Fig. 8, but with the amount of the forward sweep increased to 50 degrees. Figure 16 (a) shows the spectrum of inlet pressure fluctuation. The rotational frequency is $f_N = 66.7Hz$. We observe conventional rotating cavitation around 94Hz ($f/f_N = 1.41$) for the entire range of cavitation number shown. Alternate blade cavitation occurs around $\sigma = 0.063$. Backward rotating cavitation is found at 129Hz ($f/f_N = (-)1.95$) for $0.065 < \sigma < 0.078$. This propagation velocity ratio of –1.95 is larger than that for the three bladed inducer (-159/117=-1.36) mentioned before, and is in qualitative agreement with the theoretical results of –1.25 for four bladed inducer and –1.0 for three bladed inducer at $\sigma/2\alpha = 1.0$.

Figure 16 (b) shows the plot of the phase of inlet pressure fluctuation components at various circumferential locations denoted by θ. For the backward rotating cavitation, the phase advances as we proceed in the direction of the impeller rotation and reaches 360 degrees as we make one turn. This shows that a pressure pattern with one cell is rotating in the direction opposite to the impeller. Fig. 16 (b) also shows that the conventional rotating cavitation and the alternate blade cavitation have one and two cells respectively and that both of them are rotating in the same direction as the impeller.

So far the observations of backward rotating cavitation are limited to the above two cases. Recently, a third example was obtained at NAL in the tests to develop new inducers for LE-7A engine. A detailed analysis is now
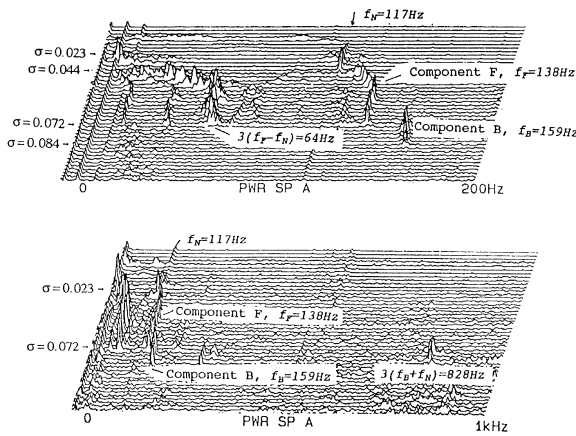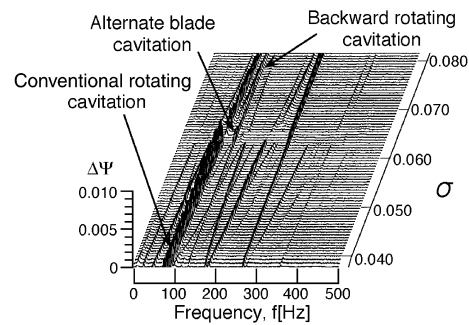

Fig. 14 Spectrum of inlet pressure fluctuations, with forward and backward rotating cavitation, from Hashimoto et al., 1997

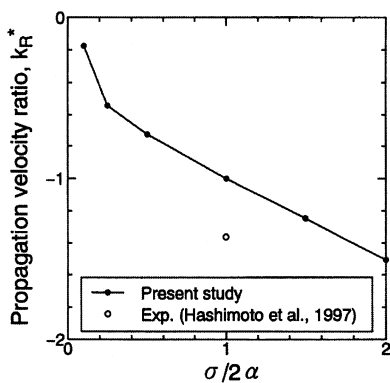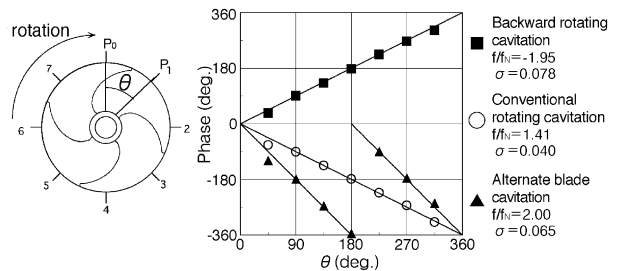(a) Spectrum of inlet pressure fluctuation

Fig. 15 Comparison of Mode IV with backward rotating cavitation, from Watanabe et al., 1999

(b) Phase (advance) of pressure fluctuation at various circumferential locations

Fig. 16 Backward rotating cavitation in a forward swept 4-bladed inducer

underway and the results will be made available in the near future.

6.3 Higher Order Rotating Cavitation (Mode VI)

Figure 17 (a) shows the spectrum of the inlet pressure fluctuation observed for a 3-bladed inducer at the rotational speed $f_N = 50Hz$. Conventional rotating cavitation is observed for $0.04 < \sigma < 0.058$, at $f_c = 61.25Hz$. In the region of cavitation number larger than that of conventional rotating cavitation onset, $0.06 < \sigma < 0.09$, we observe a component with $f_{h.o} = 250Hz$. Although hidden behind the 250Hz component, there is a component with $f_{hs} = 243.75Hz$ over $0.058 < \sigma < 0.068$. Figure 17 (b) shows the spectrum of stress fluctuation of a blade. The components with nearly constant frequency are considered to be electrical noise. With conventional rotating cavitation, for $0.04 < \sigma < 0.058$, we observe a component with $f_c - f_N = 11.25Hz$ which is the frequency of conventional rotating cavitation observed in the rotating frame. In the same way, we observe a component with $f_{ho} - f_N = 200Hz$, which is the frequency of forward propagating $f_{h.o} = 250Hz$ component observed in the rotating frame. So, this component may correspond to the higher order rotating cavitation. In the region $0.06 < \sigma < 0.068$, we observe a component with $f_{hs} = 243.75Hz$, which is the same as that observed in the inlet pressure fluctuation. This can be the higher order surge mode oscillation.

Figures 18 (a) and (b) show the phase (positive value means phase advance relative to P1 and G1) of the pressure and stress fluctuations measured at various circumferential locations. They clearly show that both conventional rotating cavitation (with 61.25Hz and 11.25Hz) and the higher order rotating cavitation (with 250Hz and 200Hz) have one cell and rotate in the direction of impeller rotation. The higher order surge mode oscillation with $f_{hs} = 243.75Hz$ has the same phase over the circumference. The frequencies of Mode VI and Mode IX (higher order rotating cavitation and higher order surge, respectively) for 3-bladed inducer observed in the stationary frame are both about 4.2 times the rotational frequency at $\sigma/2\alpha = 1.0$. This is close to the experimental values of 5.0 and 4.88 for higher order rotating cavitation and higher order surge mode oscillation respectively.

The component in Fig. 17 (a) around 240Hz observed over $\sigma > 0.075$ has low coherence between the pressure signals at different circumferential locations. For this reason, and also because it also occurs at higher inlet pressure without cavitation, we consider that the component is caused by a backflow vortex structure at the inlet.
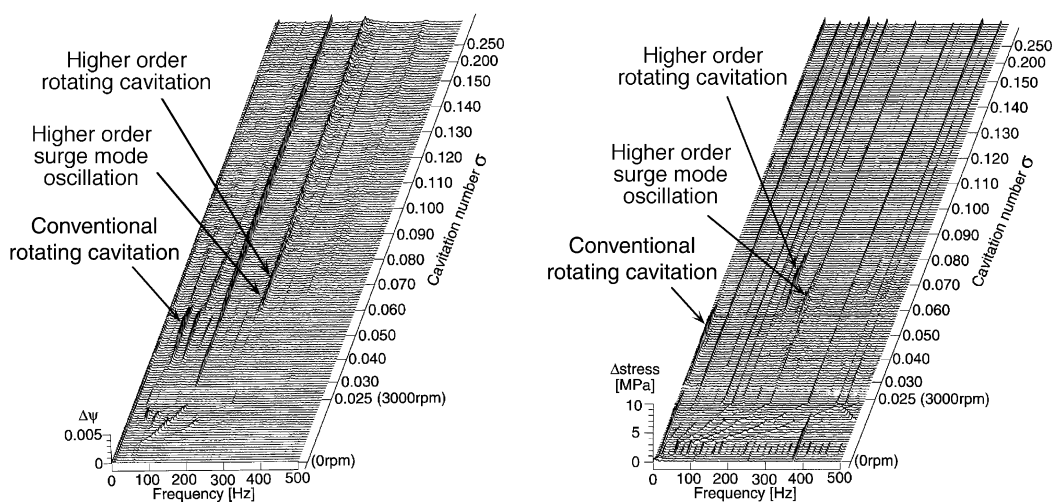
(a) Spectrum of inlet pressure fluctuation   (b) Spectrum of stress fluctuation of a blade

Fig. 17 Higher order rotating cavitation in a 3-bladed
inducer at ϕ =0.080, ψ =0.105, 3000rpm

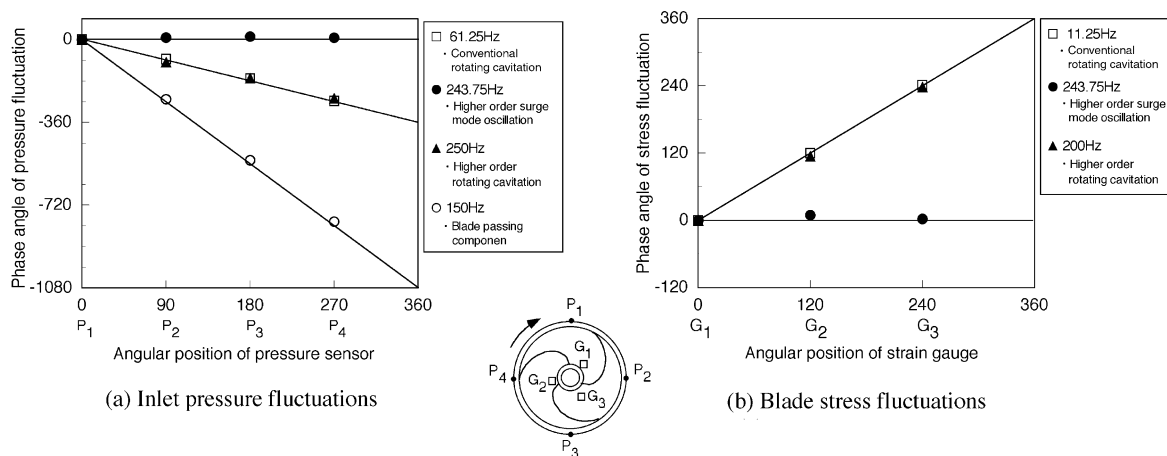Fig. 18 Phase (advance) of pressure and blade stress fluctuations shown in Fig.17

6.4 Higher Order Surge Mode Oscillation (Mode IX)

   Figures 19 (a) and (b) show the spectrum of pressure fluctuations measured at two circumferential locations separated by 90 degrees, on the casing wall and at midchord (Motoi et al., 2000).   The inducer has three blades and the rotational frequency is $f_N = 150 Hz$. We observe sharp spectrum peaks at the blade passing frequency $3 f_N$ and its harmonics.   In addition, we observe a broadband component
centered at 705Hz, which corresponds to 4.7 times the rotational frequency.   Note that the peak is higher than the blade passing component.   Figure 19 (c) and (d) show the coherence and the phase of the cross spectrum between those pressure signals.   We observe high coherence around 705Hz, and the phase difference there is zero.   This means that the 705Hz component is a surge mode oscillation.   Blade stress fluctuation has similar spectrum and has high coherence with the case pressure fluctuation around 705Hz. This component is important since the frequency is often close to that of the first bending mode of blade vibration.

   The following characteristics are found:
(1)   The frequency does not depend on the length of inlet pipe. So, it is system independent.
(2)   The onset cavitation number ($\sigma = 0.1$) is significantly larger than that of rotating cavitation ($\sigma = 0.06$).
(3)   The frequency is proportional to the rotational frequency.
   The characteristics of (1) to (3) agree with those of Mode IX.
   The Strougal number of Mode IX based on cavity length is kept nearly constant ($St = 1.3$) and the frequency changes from 3 times the rotational speed at $\sigma / 2\alpha = 0.12$ to 12 times at $\sigma / 2\alpha = 5.61$. This includes the experimental value, 4.7 times the rotational frequency, but such large dependence on $\sigma / 2\alpha$ was not identified in experiments.

  The backward rotating cavitation (Mode IV), the higher order rotating cavitation (Mode VI), and the higher order surge mode oscillation (Mode IX) introduced here are all quite repeatable for each case but they can be observed only under limited circumstances, as compared with conventional cavitation surge and rotating cavitation.   The reason for that is not known as yet.

7. CAVITY DEVELOPMENT IN ALTERNATELY CUT-BACK INDUCER

   For the purpose of suppressing rotating cavitation by promoting alternate blade cavitation, a series of tests was carried out with inducers having the leading edges of the blades alternately cut back.
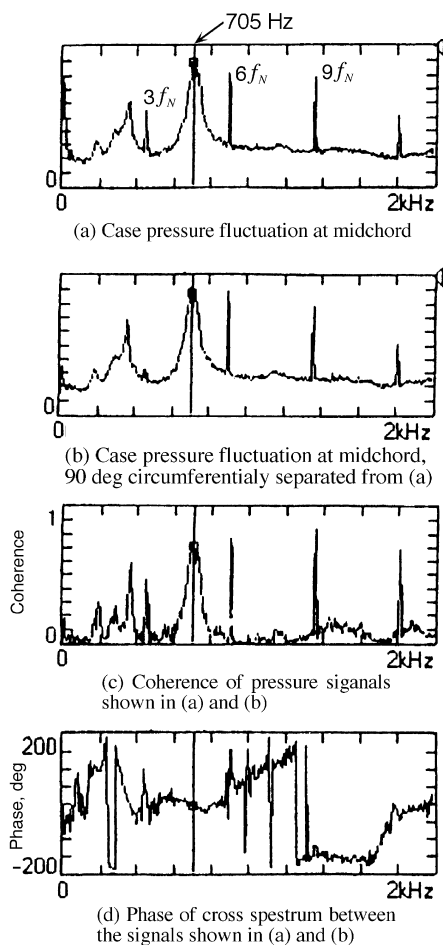
(a) Case pressure fluctuation at midchord

(b) Case pressure fluctuation at midchord, 90 deg circumferentialy separated from (a)

(c) Coherence of pressure siganals shown in (a) and (b)

(d) Phase of cross spestrum between the signals shown in (a) and (b)

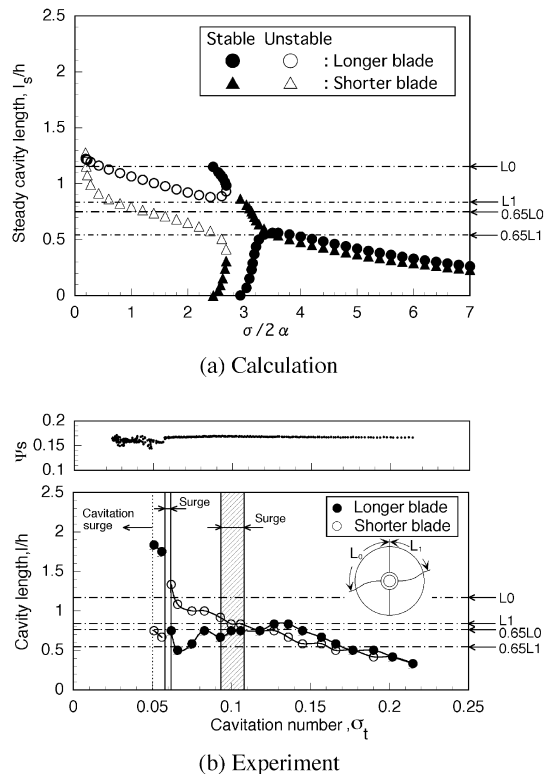Fig. 19 Higher order surge mode oscillation

(a) Calculation

(b) Experiment

Fig. 20 Cavity development in a alternately cut-back inducer 0-15, for ϕ =0.060

Figure 20 shows the results for Inducer 0-15, for which the leading edge of an unswept inducer is cut back alternately by 15 degrees at the tip. Let us focus on the analytical results of Fig.20 (a). At sufficiently larger $\sigma/2\alpha$, the cavities on longer blades are longer, as expected. As we decrease $\sigma/2\alpha$ from $\sigma/2\alpha = 7$, the cavities on both the longer and shorter blades grow, but when the length of the cavity on shorter blades reaches 65% of the spacing L1 shown in the figure, it grows more rapidly and the cavity on the longer blades becomes shorter. As a result, we have a region in which the cavities are longer for shorter blades. Next, let us consider the cavities at smaller $\sigma/2\alpha$, say $\sigma/2\alpha = 1.0$. We have longer cavities on longer blades and both cavities are longer than 0.65L0 and 0.65L1 for longer and shorter cavities respectively. As we increase $\sigma/2\alpha$, both cavities become shorter, and when the shorter cavity becomes shorter than 0.65L1 it decreases quickly and the longer cavity becomes longer. The results of the stability analysis show that the branch for smaller $\sigma/2\alpha$ is statically unstable.

Experimental results are shown in Fig.20 (b). We do have a region in which the cavities are longer for shorter blades, sandwiched by the regions with longer cavities on longer blades. Although we may need to modify the number from 65% to 90%, we believe that the strange behavior is caused by the interaction of the local flow near the cavity trailing edge with the leading edge of the neighboring blade. The two types of cavitations are shown in Fig.21. We observed surge mode oscillations around the transition points between the two types of cavitations and it proved, unfortunately, that the alternate cut back is not a good idea for stabilizing the operation of the inducer.
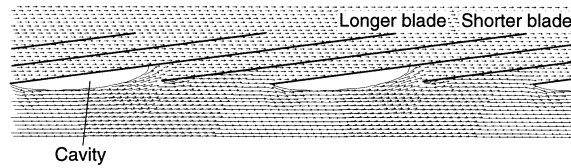
Longer cavity on longer blade
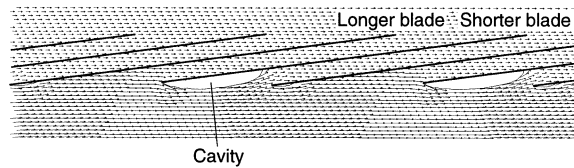
Longer cavity on shorter blade

Fig. 21 Two types of cavitation : Longer cavity on
longer blade, and longer cavity on shorter blade

8. CONCLUSION

Cavitation instabilities in turbomachines are reviewed correlating with the results of a stability analysis based on a two-dimensional linear closed cavity model.   Various modes of cavitation instabilities predicted by the analysis do occur in real machines, although generally observed instabilities are limited to cavitation surge and rotating cavitation.   It was shown that the most important factor for the cavitation instability is the steady cavity length, or $\sigma/2\alpha$, which was introduced by Acosta to represent the partial cavity length more than 40 years ago.   It should be emphasized that the cavities longer than 65-90% of the spacing are basically unstable for a number of instability modes, although real onset of instabilities is more limited than predicted by the analysis.   Since such cavities occur quite generally under normal operating conditions of rocket pump inducers, it is necessary to confirm that all possible modes are adequately suppressed under all operating conditions encountered in real flights.

References

Acosta, A.J., 1955, "A Note on Partial Cavitation of Flat Plate Hydrofoils," Calif. Inst. Of Tech. Hydro Lab. Report No. E-19.9.

Acosta, A.J., 1958, "An Experimental Study of Cavitating Inducers", Second Symposium on Naval Hydrodynamics, Washington D.C., August, pp.533-557.

Acosta, A.J., and Furuya,O., 1979 "A Brief Note on Linearized, Unsteady Supercavitating Flow," Journal of Ship Research, Vol.23, No.2, June, pp.85-88.

Acosta, A.J., Tsujimoto, Y., Yoshida,Y., Azuma, S., and Cooper, P., 2000, "Effects of Leading Edge Sweep on the Cavitating Characteristics of Inducer Pumps," Proceedings of the 8th International Symposium on Transport Phenomena and Dynamics of Rotating Machinery, ISROMAC-8, Vol.8, Honolulu, March, pp.181-188.

Arndt, R.E.A., Kjeldsen, M., and Effertz, M., 1998, "Investigation of Unsteady Cavitation Phenomena," Proceedings of US-Japan Seminar on Abnormal Flow Phenomena in Turbomachines, Osaka, November.

Arndt, R.E.A., Song, C.C.S., Kjeldsen, M., He, J., and Keller, A., 2000, "Instability of Partial Cavitation:A Numerical/Experimental Approach," Proceedings Twenty Third Symposium on Naval Hydrodynamics, Val de Reuil, Sept.

Brennen, C.E., and Acosta, A.J., 1973, "Theoretical, Quasi-Static Analysis of Cavitating Compliance in Turbopumps," Journal of Spacecraft, Vol.10, No.3, March, pp.175-179.

Brennen, C.E., and Acosta, A.J., 1976,"The Dynamic Transfer Function for a Cavitating Inducer," Journal of Fluids Engineering, Vol.98, No.2, June, pp.182-191.

Brennen, C.E., 1978,"Bubbly Flow Model for the Dynamic Characteristics of Cavitating Pumps," J. Fluid Mech., Vol.89, part 2, pp.223-240.

Brennen, C.E., Meissner, C., Lo. E.Y., and Hoffmanns, G.S., 1982, "Scale Effects in the Dynamic Transfer Functions for Cavitating Inducers," Journal of Fluids Engineering, Vol. 104, No.4, pp.428-433.

Duttweiler, M.E., and Brennen, C.E., 2000, "Surge Instability on a Cavitating Propeller" under consideration for publication in J. Fluid Mech.

Franc, J-P., 2001, "Partial Cavity Instabilities and Re-Entrant Jet" Fourth International Symposium on Cavitation, Pasadena, California, USA.

Friedrichs, J., and Kosyna, G., 2001, "Rotating Cavitation in a Centrifugal Pump Impeller of Low Specific Speed", Prceedings of Fluids Engineering Division Summer Meeting, 4th International Symposium of Pumping Machinery, May 29-June 1, 2001, New Orleans, Louisiana.

Hashimoto, T., Yoshida,M., Watanabe,M., Kamijyo,K., and Tsujimoto, Y., 1997,"Experimental Study on Rotating Cavitation of Rocket Propellant Pump Inducers," AIAA Journal of Propulsion and Power, Vol.13, No.4, pp.488-494.

Horiguchi, H., Watanabe, S., Tsujimoto, Y., and Aoki, M., 2000A, " Theoretical Analysis of Alternate Blade Cavitation in Inducers," Journal of Fluids Engineering, Vol.122, No.1, pp.156-163.

Horiguchi, H., Watanabe, S., and Tsujimoto, Y., 2000B, "A Linear Stability Analysis of Cavitation in a Finite Blade Count Impeller," Journal of Fluids Engineering, Vol.122, No.4, pp.798-805

Ihara, A., Watanabe, H., and Shizukuishi, F., 1989, "Experimental Research on the Effects of Sweep on Unsteady Hydrofoil Loading in Cavitation", Journal of Fluids Engineering, Vol.111, No.3, pp.263-269.

Kim, J.H., and Acosta, A.J., 1975 "Unsteady Flow in Cavitating Turbopumps," Journal of Fluids Engineering, Vol.96, No.3, December, pp.412-418.

Kjeldsen, M., Arndt, R.E.A., and Effertz, M., 2000, "Spectral Characteristics of Sheet/Cloud Cavitation", Journal of Fluids Engineering, Vol.122, No.3, pp. 481-487.

Motoi, H., Oguchi, H., Hasegawa,K., Miyagawa, K., Nakatsuji, H., Uchiumi, M., Hashimoto, T., Horiguchi,H., and Tsujimoto, Y., 2000, " Higher order Cavitation Surge in a Inducer and Resulting Stress Fluctuation," Proceedings of the 45th Meeting of Turbomachinery Society of Japan (in Japanese), Hachinohe, Sept.

Otsuka, S., Tsujimoto, Y., Kamijyo, K., amd Furuya,O., 1996, "Frequency Dependence of Mass Flow Gain Factor and Cavitation Compliance of Cavitating Inducers,", Journal of Fluids Engineering, Vol.118, No.3, pp. 400-408.

Pham, T.M., Larrarte, F., and Fruman., D.H., 1988, "Investigation of Unstable Cloud Cavitation," Third International Symposium on Cavitation, Vol.1,Grenoble, pp.215-220.

Tsujimoto, Y., Kamijo, K., and Yoshida,Y., 1993,"A Theoretical Analysis of Rotating Cavitation in Inducers," Journal of Fluids Engineering, Vol. 115, No.1, pp.135-141.

Tsujimoto, Y., Yoshida, Y., Maekawa, M., Watanabe, S., and Hashimoto, T., 1997, "Observations of Oscillating Cavitations of an Inducer," Journal of Fluids Engineering, Vol.119, No.4, pp.775-781.

Tsujimoto, Y., Yoshida, Y., Kataoka, D., and Horiguchi, H., 2000," Effects of Alternate Blade Length on Unsteady Cavitation in 4-Bladed Inducers (1st Report, In Case of Weak Unevenness)'" Trans. JSME, Ser.B, Vol.66, No.645, pp.1331-1319.

Watanabe, S., Tsujimoto, Y., Franc, J-P., and Michel, J-M., 1998,"Linear Analyses of Cavitating Instabilities," Proceeding of 3rd International Symposium on Cavitation, Vol.1,   Grenoble, pp.347-352.

Watanabe, S., Sato,K., Tsujimoto, Y., and Kamijo, K., 1999, "Analysis of Rotating Cavitation in a Finite Pitch Cascade Using a Closed Cavity model and a Singularity Method," Journal of Fluids Engineering, Vol.121, No.4, pp.834-840.

Watanabe, S., Tsujimoto, Y., and Furukawa, A., 2000, "Theoretical Analysis of Transitional and Partial Cavity Instabilities," Proceedings of ASME FEDSM'00, Boston.